Continuation of Nonsmooth Bifurcations in Filippov Systems Using Singular Point Tracking

Iván Arango and John Alexander Taborda

Abstract—In this paper, we propose a novel numerical method for continuation of nonsmooth bifurcations in discontinuous piecewise smooth systems or Filippov systems which we are denominated Singular Point Tracking (SPT). We use the evaluation of the vector fields on the discontinuity boundary (DB) to analyze the dynamics of the systems without integration of the ODE sets or integrating only in the points computed by the SPT algorithm. We apply a classification of points and events on DB recently proposed. Local and global nonsmooth bifurcations are detected using the SPT method. Two principal advantages have the SPT method with other numerical methods to continuation of bifurcations in nonsmooth systems. First, the integration-free algorithms in the SPT avoid the well know numerical problems of these algorithms. Second, when the integration is unavoidable the SPT method computes the initial condition of the simulation to reduce the compute time. A piecewise smooth prey-predator model is used as illustrative example of the SPT method.

Keywords—Bifurcation theory, continuation techniques, filippov systems, nonsmooth bifurcations.

I. INTRODUCTION

NONSMOOTH characteristics as sliding, switching or impact cause many mathematical and numerical difficulties in modeling, simulation and analysis stages [1-4]. The bifurcation theory and the piecewise smooth approach have been used widely to analyze the dynamics of nonsmooth systems as power converters [5,6], friction oscillator [7-9], impact oscillators [10-12] or ecological models [13,14].

The focus of this paper is in the discontinuous piecewise smooth systems (PWS) or Filippov systems. A lot of papers have been restricted to continuous PWS systems or Filippov systems not involving sliding motion because of the analysis is more simplified [15,16]. When the sliding motion on the discontinuity boundary is possible, the analysis is more complicated.

The number of specialized software in nonsmooth dynamics is reduced [17,18]. In [19] and [20,21], they are presented two toolboxes for analysis and continuation of nonsmooth

bifurcations in Filippov systems. In this paper, we propose a novel numerical method for continuation of nonsmooth bifurcations which we are denominated: *Singular Point Tracking (SPT)*.

We use the evaluation of the vector fields on the discontinuity boundary (DB) to analyze the dynamics of the Filippov systems without integration of the ODE sets or integrating only in the points computed for the SPT algorithm. We apply a classification of forty-one points and seven events on DB recently proposed in [22-24]. The existence conditions of the two crossing points (C class), the four non-singular sliding points (S class) and the thirty-five singular sliding points (Ω class) are formulate using *Boolean-valued functions* B(.) based on integration-free geometric criterions. These conditions are easily programmable and they can be used directly in the detection of nonsmooth bifurcations

The existence of singular sliding points on DB determines the existence of the events on DB and the change of the event type when a parameter is varied determines the existence of nonsmooth bifurcations. Therefore, a continuation technique of nonsmooth bifurcations can be defined tracking the singular points on DB under variation in the parameters. Local and global nonsmooth bifurcations are detected using SPT method.

Two principal advantages have the SPT method with other numerical methods to continuation of bifurcations in nonsmooth systems. First, the integration-free algorithms in the SPT avoid the well know numerical problems of these algorithms. Second, when the integration is unavoidable the SPT method computes the initial condition of the simulation to reduce the compute time.

The paper is organized as follows. In section II we present the background concepts of Filippov systems. The type of points and events on DB are summarized in the sections III and IV, respectively. In the sections V and VI we present the SPT method to continuation of local and global nonsmooth bifurcation in Filippov systems, respectively. An illustrative example based on ecological models is presented in the section VII. Finally, the conclusions and future work are discussed in the section VIII.

II. BACKGROUND

The Filippov systems are systems with discontinuous vector fields. These systems are characterized by the presence of the discontinuity boundaries in the phase space between regions where the vector field is smooth and continuous. The system flow can be expressed as:

$$\dot{x} = \begin{cases} F_i(x,\alpha) & for \quad Z_i \\ F_j(x,\alpha) & for \quad Z_j \end{cases} \tag{1}$$

where F_i and F_j are sufficiently smooth vector functions; Z_i and Z_j are the corresponding smooth phase space and $\alpha \in R$ is the parameter. These zones depend of the scalar function of the scalar function $H(x,\alpha)$ and they are defined in the equation (2).

$$\begin{cases} Z_i := \{x \in R^n : H(x,\alpha) > 0\} \\ Z_j := \{x \in R^n : H(x,\alpha) < 0\} \end{cases} \tag{2}$$

Between Z_i and Z_j, the system has the discontinuity boundary (DB) that it is assumed to be a smooth hyperplane. The DB is denoted as Σ and it is defined in the equation (3).

$$\Sigma := \{x \in R^n : H(x,\alpha) = 0\} \tag{3}$$

The system (1) is not invertible because of the orbits can overlap on DB with sliding [16]. In sliding situations, a convex combination $G(x,\alpha)$ of the vectors F_i and F_j is defined as the Filippov Method [15]. The vector G can be written as the equation (4) where λ is a parameter defined in function of the vector fields projections in the tangent vector H_t defined as $F_i^t = \langle H_t, F_i \rangle$ and $F_j^t = \langle H_t, F_j \rangle$ where $\langle \cdots, \cdots \rangle$ denotes scalar product.

$$G(x,\alpha) = \lambda F_i(x,\alpha) + (1-\lambda) F_j(x,\alpha) \tag{4}$$

with $\lambda = \dfrac{\langle H_t(x), F_j(x) \rangle}{\langle H_t(x), F_j(x) - F_i(x) \rangle}$.

The projection of $G(x,\alpha)$ with the tangent vector: $G_t = \langle H_t, G \rangle$ is used to define the direction of sliding motion just as presented in the equation (5).

$$\begin{aligned} M_R = True \quad if \quad G_t(x_b) > 0 \\ M_L = True \quad if \quad G_t(x_b) < 0 \end{aligned} \tag{5}$$

Recently, a methodology to study nonsmooth bifurcations on DB was proposed [22-24]. In this work, with reference to

H_t, the angles of vector fields φ_i and φ_j are computed in anticlockwise direction. The conditions of each type of points on DB are defined evaluating the angles φ_i and φ_j in the analysis point $x_b \in \Sigma$. Two principal angle ranges are defined: $\Theta_J = \{\theta \in (\Delta_\theta; 180 - \Delta_\theta)\}$ and $\Theta_I = \{\theta \in (180 + \Delta_\theta; 360 - \Delta_\theta)\}$ where Δ_θ is the tolerance angle. These ranges are used to study the points on DB just as presented in the figure 1 (a). Auxiliary angle ranges are necessary to characterize the singular sliding points on DB (see figure 1 (b)).
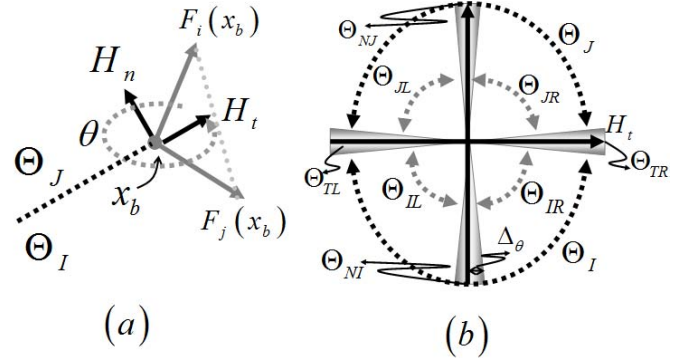

Fig. 1 Evaluation of vector fields in the analysis point x_b on DB. (a) principal angle ranges Θ_I y Θ_J. (b) Auxiliary angle ranges Θ_{TL}, Θ_{JL}, Θ_{NJ}, Θ_{JR}, Θ_{TR}, Θ_{IL}, Θ_{NI}, Θ_{IR}.

In the next section, we summarize the characterization of points on DB proposed in [22]. The numerical method Singular Point Tracking is based on this approach.

III. TYPE OF POINTS ON DISCONTINUITY BOUNDARY (DB)

Three types of points can be distinguished on the discontinuity boundary (DB): Crossing points (C), Sliding points (S) and Singular sliding points (Ω). Forty-one different points are characterized using *Boolean-valued functions* B(.) that return *True* or *False* when their arguments are evaluated. In these functions we use the logical connectives AND, OR and NOT denoted by $\wedge$, $\vee$ and $\neg$, respectively.

The *Boolean-valued conditions* B(.) for the three types of points on DB are presented in the equation (6) where $F_i^n = \langle H_n, F_i \rangle$ and $F_j^n = \langle H_n, F_j \rangle$ are the vector field projections in the normal vector H_n and Q is the condition for *pseudo-equilibrium* points given by the equation (7).

$$\begin{cases} C = B\left(F_i^n F_j^n > 0\right) \\ S = B\left(F_i^n F_j^n < 0\right) \wedge \left(\neg Q\right) \\ \Omega = B\left(F_i^n F_j^n = 0\right) \vee Q \end{cases} \tag{6}$$

$$Q = B\left(\left(180^o - \Delta_\theta\right) < |\varphi_i - \varphi_j| < \left(180^o + \Delta_\theta\right)\right) \tag{7}$$
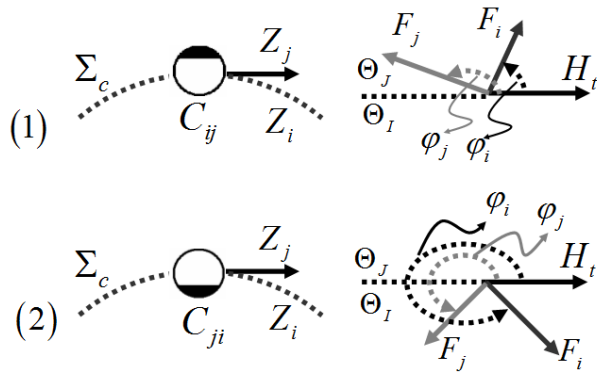
Fig. 2 Crossing points. (a) C_{ij} point: the angles φ_i and φ_j are contained in the range Θ_J. (b) C_{ji} point: the angles φ_i and φ_j are contained in the range Θ_I. Numerical codes: $N(C_{ij})=1$ and $N(C_{ji})=2$.

Crossing and sliding flows are the predominant behaviors of the Filippov systems on the discontinuity boundary (DB). Depending of the direction of the crossing orbits, two crossing (C) points are defined and four sliding (S) points are determined depending of the stability and the sliding motion direction. The thirty-five singular sliding points (Ω) exist in the transition of C and S points on DB.

A. Crossing Points (C):

In the equation (8) we present the Boolean-valued conditions B(.) for the crossing points C_{ij} and C_{ji}. Both vector field angles φ_i and φ_j should be contained in the same range Θ_I or Θ_J. The symbols, the angular evaluations and the numerical codes $N(x_b)$ for each crossing point are presented in the figure 2.

$$\begin{cases} C_{ij} = C \wedge B\left(\varphi_i \in \Theta_J\right) \wedge B\left(\varphi_j \in \Theta_J\right) \\ C_{ji} = C \wedge B\left(\varphi_i \in \Theta_I\right) \wedge B\left(\varphi_j \in \Theta_I\right) \end{cases} \qquad (8)$$
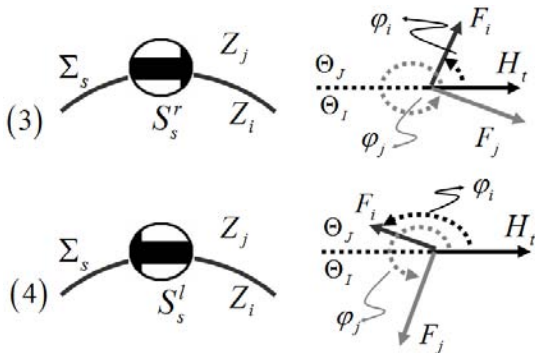
Fig. 3 Nonsingular sliding points (Stable sliding points): the angle φ_i is contained in the range Θ_J and the angle φ_j is contained in the range Θ_I. (a) M_R is *True*. (b) M_L is *True*. Numerical codes: $N(S_s^r)=3$ and $N(S_s^l)=4$.

B. Sliding Points (S):

In the sliding points we characterize stability and direction of the sliding orbits. A sliding (S) point is stable if the

Boolean-valued function S_s presented in the equation (9) is *True*.

$$S_s = S \wedge B\left(\varphi_i \in \Theta_J\right) \wedge B\left(\varphi_j \in \Theta_I\right) \qquad (9)$$

In the same form, a sliding (S) point is unstable if the Boolean-valued function S_u presented in the equation (10) is *True*. Note that each B(.) function is excluding for each analysis point x_b, i.e. if $C_{ij}(x_b)$ is *True* then C_{ji}, S or Ω are *False* in this point. Also, if S_s is *True* in a point on DB then S_u is *False*.

$$S_u = S \wedge B\left(\varphi_i \in \Theta_I\right) \wedge B\left(\varphi_j \in \Theta_J\right) \qquad (10)$$

The sliding direction is toward H_t direction if the Boolean-valued function S^r is *True*. On the other hand, the sliding direction is toward H_t opposed direction if the Boolean-valued function S^l is *True*. These conditions are presented in the equations (11) and (12), respectively.

$$S^r = S \wedge M_R \qquad (11)$$

$$S^l = S \wedge M_L \qquad (12)$$

Therefore, the necessary and sufficient Boolean-valued conditions for the four sliding (S) points are given in the equation (13).

$$\begin{cases} S_s^l = S_s \wedge S^l & S_u^l = S_u \wedge S^l \\ S_s^r = S_s \wedge S^r & S_u^r = S_u \wedge S^r \end{cases} \qquad (13)$$

In the figures 3 and 4 we present the symbols, the angular evaluations and the numerical codes $N(x_b)$ for each nonsingular sliding point. Note that the vector field angles φ_i and φ_j are contained in the different ranges (Θ_I or Θ_J).
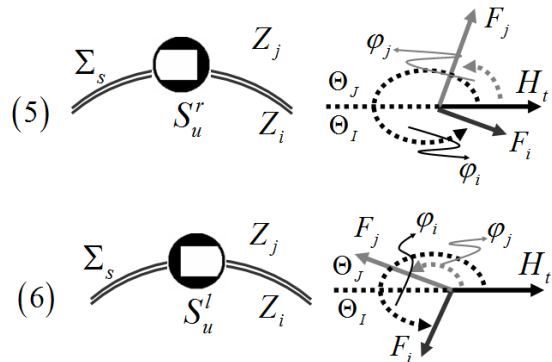

Fig. 4 Nonsingular sliding points (Unstable sliding points): the angle φ_i is contained in the range Θ_I and the angle φ_j is contained in the range Θ_J. (a) M_R is *True*. (b) M_L is *True*. Numerical codes: $N(\underline{S}_u^r)=5$ and $N(\underline{S}_u^l)=6$.

(7) (8) (9) (10)

$$T_i^{sr} \qquad T_i^{sl} \qquad T_j^{sr} \qquad T_j^{sl}$$

(11) (12) (13) (14)

$$T_i^{ur} \qquad T_i^{ul} \qquad T_j^{ur} \qquad T_j^{ul}$$
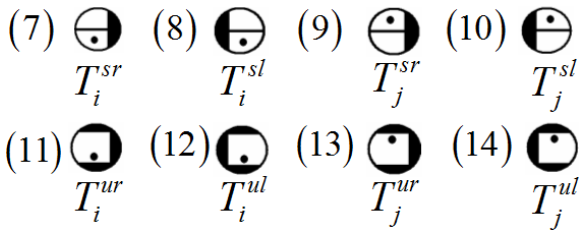
Fig. 5 Tangent (T) Singular Points. Normal component of F_i or F_j is zero. Numerical codes N(T)={7;14}.

C. Singular Sliding Points (Ω):

To analyze the singular sliding points (Ω) we define six subclasses: T, V, Π, Ψ, Q and Φ. Next, we explain the general considerations of each subclass. More details can be found in [xxx].

1) *Tangent (T) Singular Points:* The vector field F_i or F_j is tangent on the analysis point x_b.

The Boolean-valued condition for Tangent (T) singular points is given in the equation (14) where $\Theta_T=\{\Theta_{TL},\Theta_{TR}\}$ (see figure 1(b)).

$$T = B\left(\varphi_i \in \Theta_T\right) \vee B\left(\varphi_j \in \Theta_T\right) \qquad (14)$$

Eight different options are possible depending of the vector field characteristics that it is not tangent. If F_i is tangent then the characteristics of F_j define four different points: T_i^{sr}, T_i^{sl}, T_i^{ur}, T_i^{ul}. If F_j is tangent then the characteristics of F_i define four different points: T_j^{sr}, T_j^{sl}, T_j^{ur}, T_j^{ul}. In the figure 5 we present the symbols of the Tangent singular points.

2) *Vanished (V) Singular Points:* The vector field F_i or F_j is vanished on the analysis point x_b.

The Boolean-valued condition for Vanished (V) singular points is given in the equation (15) where Θ [0 °,360°].

$$V = B\left(\varphi_i \notin \Theta\right) \vee B\left(\varphi_j \notin \Theta\right) \qquad (15)$$

Again, eight different options are possible depending of the vector field characteristics that it is not vanished. If F_i is vanished then the characteristics of F_j define four different points: V_i^{sr}, V_i^{sl}, V_i^{ur}, V_i^{ul}. If F_j is vanished then the characteristics of F_i define four different points: V_j^{sr}, V_j^{sl}, V_j^{ur}, V_j^{ul}. In the figure 6 we present the symbols of the Vanished singular points.

3) *Tangent-Tangent (Π) Singular Points:* The vector fields F_i and F_j are tangent on the analysis point x_b.

The Boolean-valued condition for Tangent-Tangent (Π) singular points is given in the equation (16).
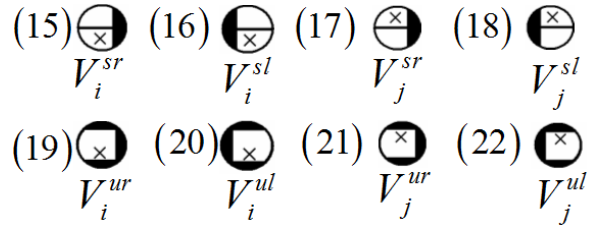
(15) (16) (17) (18)

$$V_i^{sr} \qquad V_i^{sl} \qquad V_j^{sr} \qquad V_j^{sl}$$

(19) (20) (21) (22)

$$V_i^{ur} \qquad V_i^{ul} \qquad V_j^{ur} \qquad V_j^{ul}$$

Fig. 6 Vanished (V) Singular Points. Tangent and normal components of F_i or F_j are zero. Numerical codes N(V) ={15;22}.

$$\Pi = B\left(\varphi_i \in \Theta_T\right) \wedge B\left(\varphi_j \in \Theta_T\right) \qquad (16)$$

Four different options are possible depending of the flow direction of the tangent vectors on the analysis point. If F_i and F_j are tangents toward to H_t direction then the point Π is denoted as Π_{rr}. If both vector fields are tangents toward to H_t opposed direction then the point Π is denoted as Π_{ll}. When the tangent vectors have different directions are presented the other two points denoted as Π_{rl} and Π_{lr}. In the figure 7 we present the symbols of the Tangent-Tangent (Π) singular points.

4) *Tangent-Vanished (Ψ) Singular Points: A* vector field F_i or F_j is tangent and the other vector field is vanished on the analysis point x_b.

The Boolean-valued condition for Tangent-Vanished (Ψ) singular points is given in the equation (17).

$$\begin{cases} \Psi = \Psi_1 \vee \Psi_2 \\ \Psi_1 = B\left(\varphi_i \in \Theta_T\right) \wedge B\left(\varphi_j \notin \Theta\right) \\ \Psi_2 = B\left(\varphi_i \notin \Theta\right) \wedge B\left(\varphi_j \in \Theta_T\right) \end{cases} \qquad (17)$$

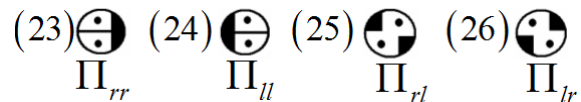(23) (24) (25) (26)

$$\Pi_{rr} \qquad \Pi_{ll} \qquad \Pi_{rl} \qquad \Pi_{lr}$$

Fig. 7 Tangent-Tangent (Π) Singular Points. Normal components of F_i and F_j are zero. Numerical codes N(Π) ={23;26}.

(27) (28) (29) (30)

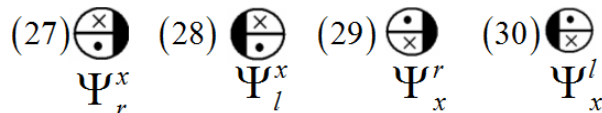$$\Psi_r^x \qquad \Psi_l^x \qquad \Psi_x^r \qquad \Psi_x^l$$

Fig. 8 Tangent-Vanished (Ψ) Singular Points. F_i or F_j is tangent and the other vector field is vanished. Numerical codes N(Ψ) ={27;30}.

Four different options are possible depending of the flow direction of the tangent vector on the analysis point. If F_i is tangent toward to H_t direction and F_j is vanished on x_b then the point Ψ is denoted as Ψ_r^x. If F_i is tangent toward to H_t opposed direction and F_j is vanished on x_b then the point Ψ is denoted as Ψ_l^x. In the other two points F_j is the tangent vector field and F_i is vanished. These points are denoted as Ψ_x^r and Ψ_x^l. In the figure 8 we present the symbols of the Tangent-

Vanished (Ψ) singular points.

5) *Quadrant (Q) Singular Points:* The vector fields F_i and F_j are anti-collinear on the analysis point x_b.

The Boolean-valued condition for Quadrant (Q) singular points or pseudo-equilibrium points was given in the equation (7).

Six different options are possible depending of the flow direction of the anti-collinear vector fields on x_b. The auxiliary angle ranges Θ_{JL}, Θ_{JR}, Θ_{IL} and Θ_{IR} presented in the figure 1(b) are used to determine the points Q. If the angle φ_i is contained in the range Θ_J, the angle φ_j is contained in the range Θ_I and Q is True then three points can be defined: Q_{jr}^{il}, Q_{jl}^{ir} and Q_{nj}^{ni}. If the angle φ_i is contained in the range Θ_I, the angle φ_j is contained in the range Θ_J and Q is *True* then three points can be defined: Q_{il}^{jr}, Q_{ir}^{jl} and Q_{ni}^{nj}. In the figure 9 we present the symbols of the Quadrant (Q) singular points.
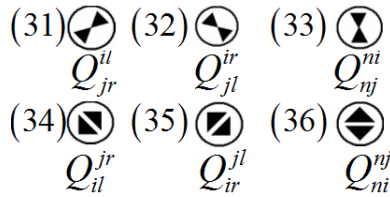
$$(31)⊙ \quad (32)⊙ \quad (33)⊙$$
$$Q_{jr}^{il} \qquad Q_{jl}^{ir} \qquad Q_{nj}^{ni}$$
$$(34)⊙ \quad (35)⊙ \quad (36)⊙$$
$$Q_{il}^{jr} \qquad Q_{ir}^{jl} \qquad Q_{ni}^{nj}$$

Fig. 9 Quadrant (Q) Singular Points. F_i and F_j are anti-collinear. Numerical codes N(Q) ={31;36}.

6) *Quadrant-Vanished (Φ) Singular Points:* A vector field F_i or F_j is vanished and the other vector field is normal to H_t on the analysis point x_b.

The Boolean-valued condition for Quadrant-Vanished (Φ) singular points is given in the equation (18) where $\Theta_N = \{\Theta_{NI}, \Theta_{NJ}\}$ (see figure 1(b)).

$$\begin{cases} \Phi = \Phi_1 \vee \Phi_2 \vee \Phi_3 \\ \Phi_1 = B(\varphi_i \notin \Theta) \wedge B(\varphi_j \notin \Theta) \\ \Phi_2 = B(\varphi_i \notin \Theta) \wedge B(\varphi_j \in \Theta_N) \\ \Phi_3 = B(\varphi_i \in \Theta_N) \wedge B(\varphi_j \notin \Theta) \end{cases} \qquad (18)$$
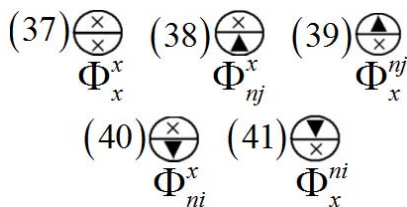
$$(37)⊗ \quad (38)⊗ \quad (39)⊗$$
$$\Phi_x^x \qquad \Phi_{nj}^x \qquad \Phi_x^{nj}$$
$$(40)⊗ \quad (41)⊗$$
$$\Phi_{ni}^x \qquad \Phi_x^{ni}$$

Fig. 10 Quadrant-Vanished (Φ) Singular Points. Tangent component F_i and F_j are zero. Numerical codes N(Φ) ={37; 41}.

Five different options are possible depending of the quadrant of the vector fields that it is not vanished on x_b. If both vector fields are vanished on x_b then the point Φ is denoted as Φ_x^x. If

F_i is normal to H_t on x_b and F_j is vanished then the direction of F_i define two points: Φ_{nj}^x and Φ_{ni}^x. If F_j is normal to H_t on x_b and F_i is vanished then the direction of F_j define two points: Φ_x^{nj} and Φ_x^{ni}. In the figure 10 we present the symbols of the Quadrant-Vanished (Φ) singular points.

IV.   TYPE OF EVENTS ON DISCONTINUITY BOUNDARY (DB)

The existence of several points types on the discontinuity boundary characterizes different scenarios on DB. Seven events are considered. In all events, a sequence of tree points is determined. The central point is a singular sliding point (Ω). The laterals points are crossing (C) points or nonsingular sliding (S) points. Let x_{b1}, x_{b2} and x_{b3} be three consecutive analysis points on DB. We assume that x_{b2} is a singular (Ω) point and we characterize the neighboring points (x_{b1} and x_{b3}). In the sections V and VI, we study the detection of singular points and their continuation techniques of local and global nonsmooth bifurcations.

1) *Change of direction in crossing orbits:*

The DB has a change of direction in crossing orbits if the Boolean-valued function Λ_{cc} presented in the equation (19) is *True*.

$$\begin{cases} \Lambda_{cc} = \Lambda_{cc1} \vee \Lambda_{cc2} \\ \Lambda_{cc1} = C_{ij}(x_{b1}) \wedge C_{ji}(x_{b3}) \\ \Lambda_{cc2} = C_{ji}(x_{b1}) \wedge C_{ij}(x_{b3}) \end{cases} \qquad (19)$$

The lateral points should be *Type C* (C_{ij} or C_{ji}) and the central point (x_{b2}) should be a singular point contained in the subsets Π or $Q^c = \{Q_{nj}^{ni}, Q_{ni}^{nj}\}$ or Φ_x^x point. The numerical codes of the central point can be N(x_{b2})={23,24,25,26,33,36,37}. An example of the event is presented in the figure 11(a).

2) *Change of crossing boundary to stable sliding boundary and vice versa:*

The DB has a change of crossing boundary to stable sliding boundary or vice versa if the Boolean-valued function Λ_{css} presented in the equation (20) is *True*.

$$\begin{cases} \Lambda_{css} = \Lambda_{css1} \vee \Lambda_{css2} \\ \Lambda_{css1} = B(x_{b1} \subset C) \wedge B(x_{b3} \subset S_s) \\ \Lambda_{css2} = B(x_{b1} \subset S_s) \wedge B(x_{b3} \subset C) \end{cases} \qquad (20)$$

The lateral points should be *Type* C={ C_{ij} ; C_{ji} } or Type $S_s = \{S_s^r ; S_s^l\}$ and the central point (x_{b2}) should be a singular point contained in the subsets $T^s = \{T_i^{sr} ; T_i^{sl} ; T_j^{sr} ; T_j^{sl}\}$, $V^s = \{V_i^{sr} ; V_i^{sl} ; V_j^{sr} ; V_j^{sl}\}$ or $\Phi^s = \{\Phi_{nj}^x ; \Phi_{ni}^x ; \Phi_x^x\}$. The numerical codes of the central point can be N(x_{b2}) = {7, 8, 9,

10, 15, 16, 17, 18, 37, 38, 41}. An example of the event is presented in the figure 11(b).

3) Change of crossing boundary to unstable sliding boundary and vice versa:

The DB has a change of crossing boundary to unstable sliding boundary or vice versa if the Boolean-valued function Λ_{cus} presented in the equation (21) is *True*.

$$\begin{cases} \Lambda_{cus} = \Lambda_{cus1} \vee \Lambda_{cus2} \\ \Lambda_{cus1} = B\left(x_{b1} \subset C\right) \wedge B\left(x_{b3} \subset S_u\right) \\ \Lambda_{cus2} = B\left(x_{b1} \subset S_u\right) \wedge B\left(x_{b3} \subset C\right) \end{cases} \quad (21)$$

The lateral points should be *Type* C={ C_{ij} ; C_{ji} } or Type S_u={S_u^{r} ; S_u^{l}} and the central point (x_{b2}) should be a singular point contained in the subsets T^u={T_i^{ur} ; T_i^{ul} ; T_j^{ur} ; T_j^{ul}}, V^u={ V_i^{ur} ; V_i^{ul} ; V_j^{ur} ; V_j^{ul} } or Φ^s={Φ_{ni}^{x} ; Φ_x^{nj} ; Φ_x^{x} }. The numerical codes of the central point can be N(x_{b2}) = {11, 12, 13, 14, 19, 20, 21, 22, 37, 39, 40}. An example of the event is presented in the figure 11(c).

4) Change of direction in stable sliding boundary:

The DB has a change of direction in stable sliding boundary if the Boolean-valued function Λ_{slr} presented in the equation (22) is *True*.

$$\begin{cases} \Lambda_{slr} = \Lambda_{slr1} \vee \Lambda_{slr2} \\ \Lambda_{slr1} = S_s^{l}\left(x_{b1}\right) \wedge S_s^{r}\left(x_{b3}\right) \\ \Lambda_{slr2} = S_s^{r}\left(x_{b1}\right) \wedge S_s^{l}\left(x_{b3}\right) \end{cases} \quad (22)$$

The lateral points should be *Type* S^s (S_s^{r} or S_s^{l}) and the central point (x_{b2}) should be a singular point contained in the subset Q^s={Q_{jr}^{il} ; Q_{jl}^{ir} ; Q_{nj}^{ni} }. The numerical codes of the central point can be N(x_{b2}) = {31, 32, 33}. An example of the event is presented in the figure 11(d).
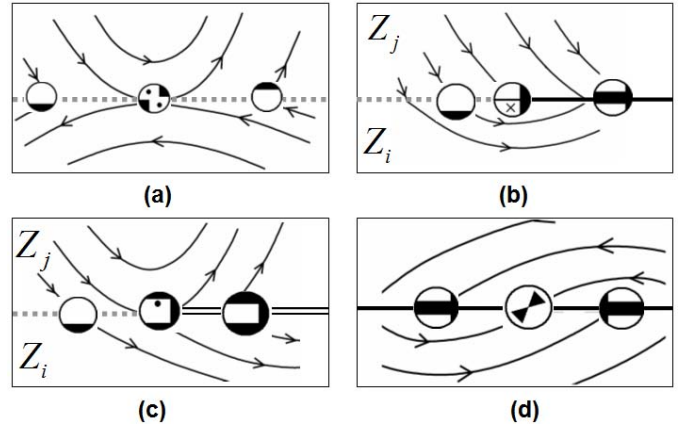
5) Change of direction in unstable sliding boundary:

The DB has a change of direction in unstable sliding boundary if the Boolean-valued function Λ_{ulr} presented in the equation (23) is *True*.

$$\begin{cases} \Lambda_{ulr} = \Lambda_{ulr1} \vee \Lambda_{ulr2} \\ \Lambda_{ulr1} = S_u^{l}\left(x_{b1}\right) \wedge S_u^{r}\left(x_{b3}\right) \\ \Lambda_{ulr2} = S_u^{r}\left(x_{b1}\right) \wedge S_u^{l}\left(x_{b3}\right) \end{cases} \quad (23)$$

The lateral points should be *Type* S^u (S_u^{r} or S_u^{l}) and the central point (x_{b2}) should be a singular point contained in the subset Q^u={Q_{ir}^{jl} ; Q_{il}^{jr} ; Q_{ni}^{nj} }. The numerical codes of the

central point can be N(x_{b2}) = {34, 35, 36}. An example of the event is presented in the figure 12(a).

(a)   **(b)**

(c)   **(d)**

Fig. 11 Examples of events on DB. (a) Event 1: C_{ji} to C_{ij}. (b) Event 2: C_{ji} to S_s^{r}. (c) Event 3: C_{ji} to S_u^{r}. (d) Event 4: S_s^{r} to S_s^{l}.

6) Change of stability in sliding boundary:

The DB has a change of stability in sliding boundary if the Boolean-valued function Λ_{us} presented in the equation (24) is *True*.

$$\begin{cases} \Lambda_{us} = \Lambda_{us1} \vee \Lambda_{us2} \\ \Lambda_{us1} = B\left(x_{b1} \subset S_s\right) \wedge B\left(x_{b3} \subset S_u\right) \\ \Lambda_{us2} = B\left(x_{b1} \subset S_u\right) \wedge B\left(x_{b3} \subset S_s\right) \end{cases} \quad (24)$$

The lateral points should be *Type* S (S^s or S^u) and the central point (x_{b2}) should be a singular point contained in the subsets Π or Ψ. The numerical codes of the central point can be N(x_{b2}) = {23, 24, 25, 26, 27, 28, 29, 30}. An example of the event is presented in the figure 12(b).

7) Change of direction in the velocity of stable sliding boundary:

The DB has a change direction in the velocity of stable sliding boundary if the Boolean-valued function Λ_{vs} presented in the equation (25) is *True*.

$$\begin{cases} \Lambda_{vs} = \left(\Lambda_{vs1} \vee \Lambda_{vs2}\right) \wedge \Lambda_{vs3} \\ \Lambda_{vs1} = S_s^{l}\left(x_{b1}\right) \wedge S_s^{l}\left(x_{b3}\right) \\ \Lambda_{vs2} = S_s^{r}\left(x_{b1}\right) \wedge S_s^{r}\left(x_{b3}\right) \\ \Lambda_{vs3} = B\left(\Delta_{Gt}\left(x_{b1}\right) > 0\right) \wedge B\left(\Delta_{Gt}\left(x_{b3}\right) < 0\right) \end{cases} \quad (25)$$

where,

$$\Delta_{Gt}\left(x_{bi}\right) = \left|G_t\left(x_{bi}\right)\right| - \left|G_t\left(x_{bi} + \delta\right)\right| \quad (26)$$

The lateral points should be *Type* S^s (S_s^{r} or S_s^{l}) and the

central point (x_{b2}) should be a singular point contained in the subset $Q^s=\{Q_{jr}^{il}\ ;\ \ Q_{jl}^{ir}\ ;\ Q_{nj}^{ni}\ \}$. The numerical codes of the central point can be $N(x_{b2}) = \{31, 32, 33\}$. An example of the event is presented in the figure 12(c).
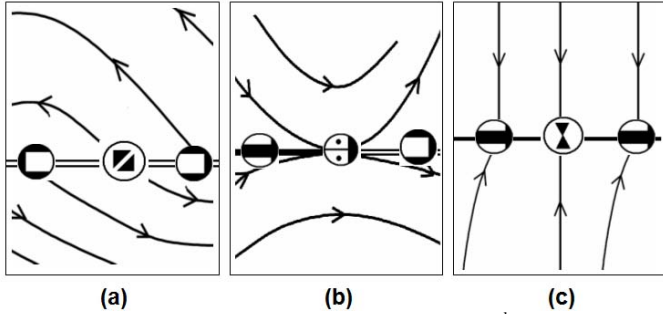

(a)   **(b)**   **(c)**

Fig. 12 Examples of events on DB. (a) Event 5: S_u^l to S_u^r. (b) Event 6: S_s^r to S_u^r. (c) Event 7: S_s^r to S_s^r.

V.   CONTINUATION OF LOCAL NONSMOOTH BIFURCATIONS USING SINGULAR POINT TRACKING (SPT)

Let n_Ω be the number of singular points on DB. Therefore, a sequence of $(2n_\Omega +1)$ points can be determined: $(x_{b1}, x_{b2},\ldots, x_{b(2n\Omega +1)})$. The points: $(x_{b1}, x_{b3},\ldots, x_{b(2n\Omega +1)})$ are crossing points ($C=\{C_{ij}; C_{ji}\}$) or nonsingular sliding points ($S=\{ S_s^r ; S_s^l ; S_u^r ; S_u^l \}$). The other points: $(x_{b2}, x_{b4},\ldots, x_{b(2n\Omega)})$ are singular points ($\Omega=\{T; V; \Pi; \Psi; Q; \Phi\}$).

Using the Boolean-valued conditions for one-event on DB given by three points (just as we explain in the previous section) is possible to characterize any combinations of events on DB considering that the laterals points (C or S) can be common to two triads of points.

The existence of singular sliding points on DB determines the existence of the events on DB. The change of the event type when the parameter α is varied determines the existence of nonsmooth bifurcations.   Therefore, a continuation technique of nonsmooth bifurcations can be defined tracking the singular points on DB under variation in the parameter α.

The first step in the SPT method consists in the determination of the initial condition in the continuation algorithm which it is reached tracking the singular points. Therefore, the parameter α is fixed and the discontinuity boundary is inspected to characterize the points and events on DB. Seven events are possible on DB. A singular point exists in each event transition. When the existence of an event is determined, the singular point is located diminishing the step size on the DB evaluation until the singular point condition is verified. In the figure 13 we present an example of singular point detection for α fixed. When the change of crossing boundary to stable sliding boundary ($C_{ji} \rightarrow S_{sl}$) is detected, the location of the tangent point T_{isl} is determined diminishing the step size.
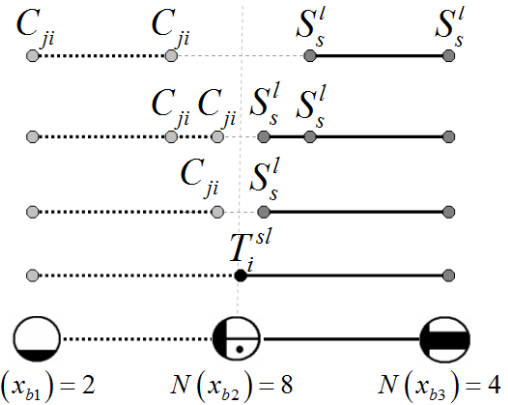

Fig. 13 Example of singular point detection for α fixed: when the event $C_{ji} \rightarrow S_s^l$ is detected, the step size is diminished until the detection of the point T_i^{sl}.

The continuation algorithm SPT has the initial condition when the three points (x_{b1},x_{b2},x_{b3}) are characterized. The numerical codes of each point $(N(x_{b1})$, $N(x_{b2})$ and $N(x_{b3}))$ are used to track the singular points when α is varied. The curves of singular points are generated computing two-dimensional points P_{ij} in the space $(x_b$ vs. α) defined as $P_{ij} := P\left(x_b(i+1),\alpha(j+1)\right)$.
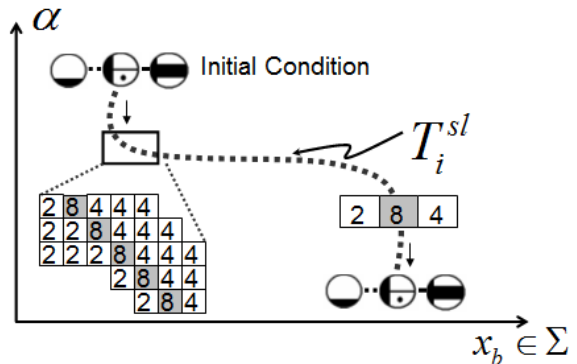

Fig. 14 Example of singular point tracking (SPT): a sequence of points $N(x_{b1},x_{b2},x_{b3})=(2,8,4)$ is used as initial condition to track the T_i^{sl} curve when α is varied.

$$\alpha(j+1) = \alpha(j)+\Delta_\alpha \quad if \quad N\left(x_b(i)\right)=N(x_{b2}) \quad (27)$$

The value of α is modified if the xb(i) component of Pij has the numerical code of the singular point N(xb2) just as we present in the equation (27) where $\Delta\alpha$ is the increment value of α.

$$x_b(i+1) = \begin{cases} x_b(i)+\Delta_x & if \quad N\left(x_b(i)\right)=N(x_{b1}) \\ x_b(i) & if \quad N\left(x_b(i)\right)=N(x_{b2}) \\ x_b(i)+\Delta_x & if \quad N\left(x_b(i)\right)=N(x_{b3}) \end{cases} \quad (28)$$

The value of   xb(i) is modified for each $\alpha(j)$ until the numerical code of $N(x_b(i))$ is equal to numerical code of the singular point $N(x_{b2})$. In the equation (28) we present the adaptation law for xb(i) where Δ_x is the increment value of xb.

In the figure 14 we present an example of singular point tracking. The T_i^{sl} curve is generated, evaluating and finding the numerical codes $N(x_{b1},x_{b2},x_{b3})=(2,8,4)$ in the space (x_b vs. α).
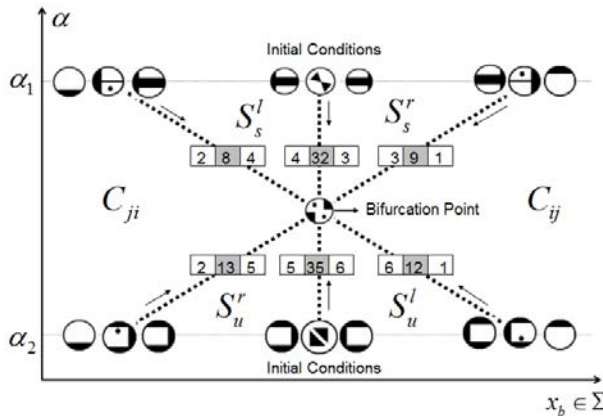

Fig. 15 Example of bifurcation point detection using SPT method: the intersection of two or more singular point curves when α is varied implies a bifurcation point.

The bifurcation points can be detected of several ways. Changes in the number of the singular points on DB or the events on DB when α is varied imply the existence of bifurcation points. Also, the intersection of two or more singular point curves implies a bifurcation point in the intersection point. In the figure 15 we present an example of bifurcation detection using SPT method. Taking as initial conditions the singular points for $\alpha=\alpha_1$ and $\alpha=\alpha_2$, the singular point curves cross in the point Π_{lr}.

In [16] the codimension-one nonsmooth bifurcations were classified. Next, we present the general consideration to detect the local nonsmooth bifurcations using the SPT method.

1) Boundary Equilibrium Bifurcations (BF,BN,BS)

The equilibrium point of the vector fields F_i or F_j can collide with the discontinuity boundary. When a hyperbolic equilibrium collides with the DB, the system has a Boundary-Equilibrium bifurcation. Depending of the equilibrium type the bifurcation is denoted as Boundary-Focus (BF), Boundary-Node (BN) or Boundary-Saddle (BS).

The BF, BN and BS bifurcations are characterized by the intersection between a tangent curve T and a pseudo-equilibrium curve Q when α is varied. In the bifurcation point the system has a singular point type V or type Φ. In the figure 16 we present two examples of boundary equilibrium bifurcations. In the figure 16(a), the BF1 bifurcation is characterized while the BN2 bifurcation is analyzed in the figure 16(b).

2) Tangent Collisions Bifurcations (DT, VV, VI, II)

The collisions of two tangent points when a parameter is varied are local codim 1 bifurcations. In [16] these bifurcations are classified depending the characteristics of the tangent points in the following classes: Double tangency (DT), Visible-Visible tangencies (VV), Visible-Invisible tangencies (VI) and Invisible-Invisible tangencies (II). To detect these bifurcations we can track the tangent curves T and determine the bifurcation point when a point type Π or Ψ is detected. In the figure 16(c) we present an example of VI1 bifurcation.

3) Pseudo-saddle-node Bifurcation (PSN)

Two pseudo-equilibrium points (type Q) can collide and disappear via the standard saddle-node bifurcation and it is known as pseudo-saddle-node (PSN) bifurcation. With the SPT method we can track the points Q and detect the intersection or the disappearance of the points when α is varied. In the figure 16(d) we present the characterization of the PSN bifurcation.
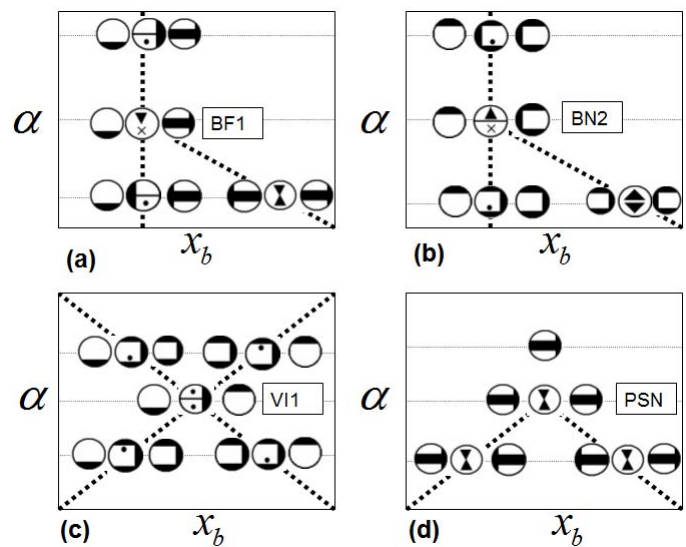

Fig. 16 Examples of continuation local nonsmooth bifurcations using SPT. (a) Boundary focus bifurcation. (b) Boundary node bifurcation. (c) Collision of visible and invisible tangencies. (d) Pseudo-saddle-node bifurcation.

VI. CONTINUATION OF GLOBAL NONSMOOTH BIFURCATIONS USING SINGULAR POINT TRACKING (SPT)

All nonsmooth bifurcations in Filippov systems can be classified as Local and Global bifurcations [16]. The local bifurcations can be detected and continued with the integration-free SPT procedure detailed in the previous section.

To analyze global bifurcations which involve sliding on the discontinuity boundary the integration is unavoidable, however using the integration-free algorithms explained in the

Section V, we can determine the initial condition of the integration to reduce the compute time. Also, in several cases with the SPT method we can integrate only a vector field to avoid numerical problems very common in simulation of nonsmooth systems.
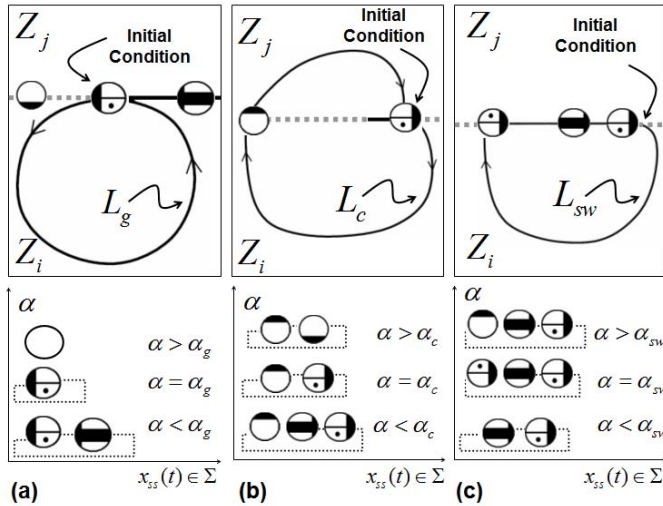

Fig. 17 Examples of continuation global nonsmooth bifurcations using SPT. (a) Grazing bifurcation. (b) Crossing bifurcation. (c) Switching bifurcation.

In Filippov systems, the periodic solutions or cycles can be divided in standard, sliding or crossing cycles. In the standard cycles, the flow lies entirely in Z_i or Z_j zone without points on DB. The sliding cycles have stable sliding points (S_s^r or S_s^l) and singular points on DB and the crossing cycles have crossing points (C_{ij} or C_{ji}) or singular points on DB.

1) Grazing Bifurcations (or Touching Bifurcations)

The Filippov system has a grazing bifurcation point when a standard cycle collides with the DB in a tangent point T_w. The tangent point should be contained in the subset $T^s = \{T_i^{sr}$; T_i^{sl} ; T_j^{sr} ; $T_j^{sl}\}$.

In the grazing transition, the Filippov system has the sequence of cycles presented in the equation (29), where L_{st} denotes a standard cycle, L_g denotes a grazing cycle and L_s denotes a sliding cycle.

$$\underbrace{L_s}_{\alpha < \alpha_G} \rightarrow \underbrace{L_g}_{\alpha = \alpha_G} \rightarrow \underbrace{L_{st}}_{\alpha > \alpha_G} \tag{29}$$

Therefore, analyzing only the points on DB in the stationary state $x_{ss}(t)$, in the cycle L_{st} there is not points on DB, in the cycle L_g there in one point on DB: T_w. Finally, in the cycle L_s two different type of points on DB can be distinguished: S and T. In the figure 17(a), we present the sequence of points on DB in the grazing transition.

The grazing condition on DB is presented in the equation

(30) where α_G is the critic value of α; n_T is the number of tangent points and t_σ is the period of the L_g cycle.

$$\begin{cases} x(t_0, \alpha_G) = T_w \subset T \in \Sigma \\ \quad x(t_1, \alpha_G) = T_w \\ \quad x(t, \alpha_G) \notin \{C, S\} \end{cases} \tag{30}$$

with $w = 1, \cdots, n_T$ $\quad t_0 \leq t \leq t_1 := t_\sigma$.

The initial condition $x(t_0)$ of the orbit is the tangent point T_w. If the tangent vector field in T_w is F_i (points: T_i^{sr} or T_i^{sl}) then we integrate the equation $\dot{x} = F_i(x, \alpha_G)$. Otherwise, if the tangent vector field in T_w is F_j (points: T_j^{sr} ; T_j^{sl}) then we integrate the equation $\dot{x} = F_j(x, \alpha_G)$. In a time t_σ the solution $x(t)$ returns to the tangent point T_w without other points on DB. In the figure 17(a), we present an example of cycle L_g for the grazing condition.

2) Crossing Bifurcations

The crossing bifurcation point happens when a crossing cycle returns to tangent point without sliding points on DB. Both field vectors F_i and F_j should be integrated to verify the crossing bifurcation. The crossing condition is presented in the equation (31) where α_C is the critic value of α.

$$\begin{cases} x(t_0, \alpha_C) = T_w \subset T \in \Sigma \\ x(t_1, \alpha_C) = C_w \subset C \in \Sigma \\ \quad x(t_2, \alpha_C) = T_w \\ \quad x(t, \alpha_C) \notin \{S\} \end{cases} \tag{31}$$

with $w = 1, \cdots, n_T$ $\quad t_0 \leq t \leq t_2 := t_\sigma$.

The initial condition $x(t_0)$ of the crossing orbit is the tangent point T_w. If the tangent vector field in T_w is F_i (points: T_i^{sr} or T_i^{sl}) then first we integrate the equation $\dot{x} = F_i(x, \alpha_C)$ and when the solution arrives to DB we integrate the equation $\dot{x} = F_j(x, \alpha_C)$. In a time t_σ the crossing cycle $x(t)$ returns to the tangent point T_w without sliding points on DB. In the figure 17(b), we present an example of cycle L_c for the crossing condition.

When α is varied, this bifurcation can be studied detecting the point on DB in the periodic solutions. Only for $\alpha = \alpha_C$ the equation (31) is hold. For $\alpha < \alpha_C$ the periodic solution has stable sliding points on DB and for $\alpha > \alpha_C$ the crossing cycle has not the tangent point T_w.

3) Switching Bifurcations (or Buckling Bifurcations)

In the switching bifurcation point the solution travels an

entire stable sliding segment and returns to a tangent point defined as initial condition T_1. Two tangent points T_1 and T_2 are necessary in the switching bifurcation. The initial condition T_1 is defined depending of the sliding segment direction just as presented in the equation (32).

$$\begin{cases} T_2 \to S_s^r \to T_1 & T_1 = T_2 \in \left\{ T_i^{sr}, T_j^{sr} \right\} \\ T_1 \to S_s^l \to T_2 & T_1 = T_2 \in \left\{ T_i^{sl}, T_j^{sl} \right\} \end{cases} \quad (32)$$

The switching condition on DB is presented in the equation (33) where α_{sw} is the critic value of α.

$$\begin{cases} x\left(t_0, \alpha_{SW}\right) = T_1 \subset T \in \Sigma \\ x\left(t_1, \alpha_{SW}\right) = T_2 \subset T \in \Sigma \\ \quad x\left(t_2, \alpha_{SW}\right) = T_1 \\ \quad x\left(t, \alpha_{SW}\right) \notin \left\{ C \right\} \end{cases} \quad (33)$$

with $t_0 \le t \le t_2 := t_\sigma$.

The tangent points T_1 and T_2 are the same type just is shown in the equation (32). If the tangent vector field in the tangent points is F_i (points: T_i^{sr} or T_i^{sl}) then we integrate the equation $\dot{x} = F_i(x, \alpha_{SW})$. Otherwise, if the tangent vector field in the tangent points is F_j (points: T_j^{sr} ; T_j^{sl}) then we integrate the equation $\dot{x} = F_j(x, \alpha_{SW})$. The solution x(t) arrives of T_1 to T_2 in a time t_1, after the solution slides and returns to T_1 in a time t_2 without crossing points on DB. In the figure 17(c), we present an example of cycle L_{sw} for the switching condition.
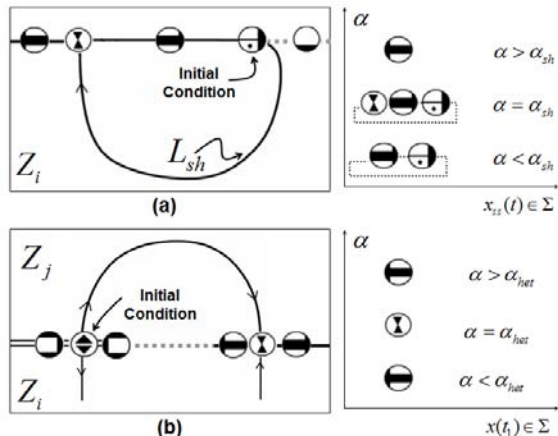

Fig. 18 Examples of continuation global nonsmooth bifurcations using SPT. (a) Pseudo-homoclinic bifurcation. (b) Pseudo-heteroclinic bifurcation.

The cycle points on DB in the stationary state $x_{ss}(t)$ when α is varied are presented in the figure 17(c). For $\alpha < \alpha_{SW}$ the periodic solution has the following points on DB: S_s (S_s^r or S_s^l) and one tangent point T_1. For $\alpha = \alpha_{SW}$ the periodic solution

has the following points on DB: S_s (S_s^r or S_s^l) and two tangent points (T_1 and T_2). Finally, for $\alpha > \alpha_{SW}$ the periodic solution has the following points on DB: S_s (S_s^r or S_s^l), crossing points (C_{ij} or C_{ji}) and one tangent point T_1.

4) Pseudo-homoclinic Bifurcations

The pseudo-homoclinic bifurcation point happens when a sliding cycle returns to tangent point without crossing points on DB via pseudo-equilibrium point. Therefore, one tangent point Tw and one stable pseudo-equilibrium point contained in the subset $Q^s = \{Q_{jr}^{il}$; Q_{jl}^{ir} ; $Q_{nj}^{ni}\}$ are necessary in the pseudo-homoclinic bifurcation. The sliding homoclinic orbit condition is presented in the equation (34) where α_{SH} is the critic value of α.

$$\begin{cases} x\left(t_0, \alpha_{SH}\right) = T_w \subset T \in \Sigma \\ x\left(t_1, \alpha_{SH}\right) = Q_w \subset Q_s \in \Sigma \\ \quad x\left(t_2, \alpha_{SH}\right) = T_w \\ \quad x\left(t, \alpha_{SH}\right) \notin \left\{ C \right\} \end{cases} \quad (34)$$

with $w = 1, \cdots, n_T \quad t_0 \le t \le t_2 := t_\sigma$.

The initial condition $x(t_0)$ of the sliding homoclinic orbit is the tangent point T_w. If the tangent vector field in the tangent points is F_i (points: T_i^{sr} or T_i^{sl}) then we integrate the equation $\dot{x} = F_i(x, \alpha_{SH})$. Otherwise, if the tangent vector field in the tangent points is F_j (points: T_j^{sr} ; T_j^{sl}) then we integrate the equation $\dot{x} = F_j(x, \alpha_{SH})$. The solution x(t) arrives of T_w to Q point in a time t_1, after the solution slides and returns to T_w in a time t_2 without crossing points on DB. In the figure 18(a), we present an example of cycle L_{sh} for the pseudo-homoclinic condition.

5) Pseudo-heteroclinic bifurcations

The pseudo-heteroclinic bifurcation point happens when two pseudo-equilibrium points are connected. Two pseudo-equilibrium points Q_1 and Q_2 are necessary for this bifurcation, one point should be contained in the subset $Q^s = \{Q_{jr}^{il}$; Q_{jl}^{ir} ; $Q_{nj}^{ni}\}$ and the other point should be contained in the subset $Q^u = \{Q_{ir}^{jl}$; Q_{il}^{jr} ; $Q_{ni}^{nj}\}$.

The heteroclinic orbit condition is presented in the equation (35) where α_{HT} is the critic value of α. Taking as initial condition $x(t_0)$ the Q point contained in Q^u, we should integrate the vector fields F_i and F_j until arrive to the DB in a time t_1. If $x(t_1)$ is a Q^s point then the equation (35) is verified.

$$\begin{cases} x\left(t_0, \alpha_{HT}\right) = Q_1 \subset Q^u \in \Sigma \\ x\left(t_1, \alpha_{HT}\right) = Q_2 \subset Q^s \in \Sigma \\ \quad x\left(t, \alpha_{HT}\right) \notin \left\{ C, S \right\} \end{cases} \quad (35)$$

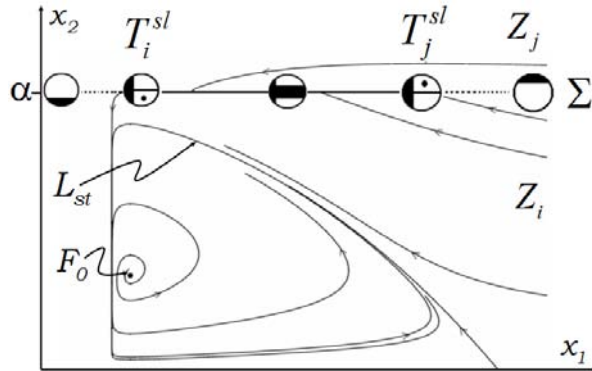In the figure 18(b) we present an example of heteroclinic bifurcation.

Fig. 19 State portrait of PWS prey-predator for α=2.75. Standard cycle (L_{st}) and unstable focus in F_0=(0.047;1.01017). Equation (38).

VII. ILLUSTRATIVE EXAMPLE: PIECEWISE SMOOTH PREY-PREDATOR MODEL

In this section, we explain the SPT method in continuation of local and global nonsmooth bifurcations by means of piecewise-smooth (PWS) prey-predator example proposed in [16].

The configuration (F_i,F_j,H) of the PWS prey-predator is presented in the equation (36) where α is the bifurcation parameter and k_1, k_2, k_3 and k_4 are the system parameters that we have assumed constants.

$$F_i(x) = \begin{pmatrix} x_1(1-x_1) - (k_1 x_1/(k_2+x_1))x_2 \\ (k_1 x_1/(k_2+x_1))x_2 - k_3 x_2 \end{pmatrix}$$

$$F_j(x) = \begin{pmatrix} x_1(1-x_1) - (k_1 x_1/(k_2+x_1))x_2 \\ (k_1 x_1/(k_2+x_1))x_2 - k_3 x_2 - k_4 x_2 \end{pmatrix} \quad (36)$$

$$H(x,\alpha) = x_2 - \alpha = 0$$

The parameters k_i are fixed in the values proposed in [16] just as is presented in the equation (37).

$$\begin{cases} k_1 = 0.3556 & k_2 = 0.33 \\ k_3 = 0.0444 & k_4 = 0.2067 \end{cases} \quad (37)$$

The state variables x_1 and x_2 correspond to prey density and predator density, respectively. These densities should be positive $x_1 > 0$ and $x_2 > 0$. In the state portraits the prey density is varied in the range $0<x_1<1$ while the predator density is considered from 0 until a little bigger than α threshold. The bifurcation parameter α is associated to the DB $\Sigma=\{x : x_2 = \alpha\}$ and α is varied in the range [3; 0.25].
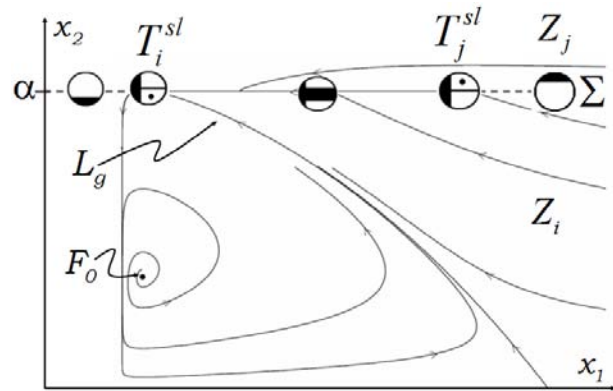

Fig. 20 State portrait of PWS prey-predator for α ≈ 2.44. Grazing bifurcation: The cycle L_g grazes the DB in the tangent point.

First, we analyze with SPT method the prey-predator system for different decreasing values of α. Later, we apply the continuation techniques for local and global nonsmooth bifurcations based on SPT method.

For values of α near to 3, the analysis of prey-predator system on DB has the sequence of points presented in the equation (38). Two singular points are detected: T_i^{sl}=(0.047;α) and T_j^{sl}=(0.793;α). The singular points are in the transitions of two changes of crossing boundary to stable sliding boundary explained in the Section IV(1).

$$C_{ji} \rightarrow \underbrace{T_i^{sl}}_{x_{b2x}=0.047} \rightarrow S_s^l \rightarrow \underbrace{T_j^{sl}}_{x_{b4x}=0.793} \rightarrow C_{ij} \quad (38)$$

In the figure 19, we present the state portrait x_1 vs. x_2 for α=2.75. In the zone Z_i, the vector field F_i has a unstable focus F_0 and a standard cycle L_{st}. The direction of the sliding segment S_s^l is associated to the flow direction in the cycle L_{st} and the tangent point T_i^{sl} is aligned with the focus F_0.
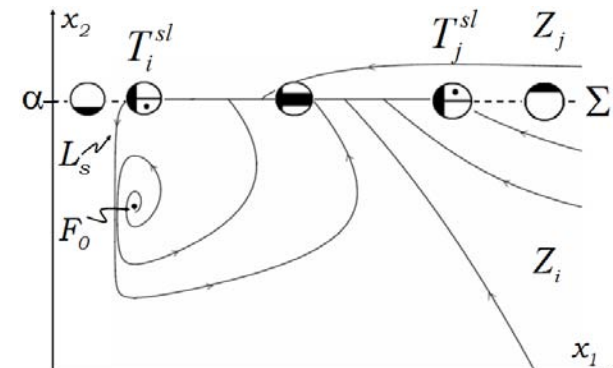

Fig. 21 State portrait of PWS prey-predator for α=1.625. Stable sliding cycle (L_s) in discontinuity boundary H=x_2 - α. Equation (38).

When α is diminished, the discontinuity boundary comes closer to the standard cycle L_{st}. For α ≈ 2.44 the standard cycle collides with the DB in the tangent point T_i^{sl}. This fact is well known as grazing bifurcation. The grazing bifurcation is

not detected with the DB analysis, however the DB information can be used to reduce the compute time in the global bifurcation detection. Using the tangent point T_i^{sl} as initial condition we integrate the vector field Fi and we verify the existence of the cycle L_g easily. In the figure 20 we present the state portrait for the critic value $\alpha \approx 2.44$.
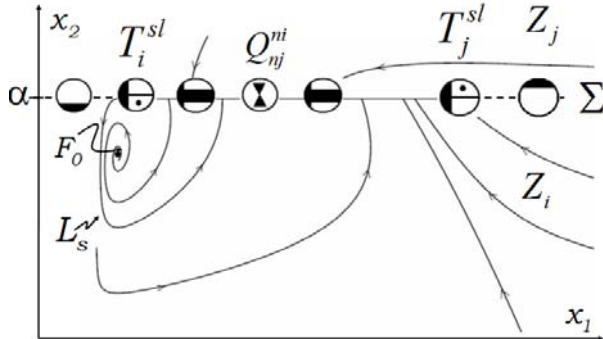

Fig. 22   State portrait of PWS prey-predator for $\alpha \approx 1.2437$. Pseudo-saddle-node bifurcation. Equation (39).

After the grazing bifurcation $\alpha < 2.44$, the periodic solution becomes in sliding cycle Ls. The sequence of points on DB is equal to the sequence given in the equation (38). In the figure 21 we present the state portrait of the PWS prey-predator for $\alpha=1.625$. The results presented in the figures 19, 20 and 21 are equivalent with the figure 17(a). The solution has a transition of standard cycle to grazing cycle to sliding cycle.
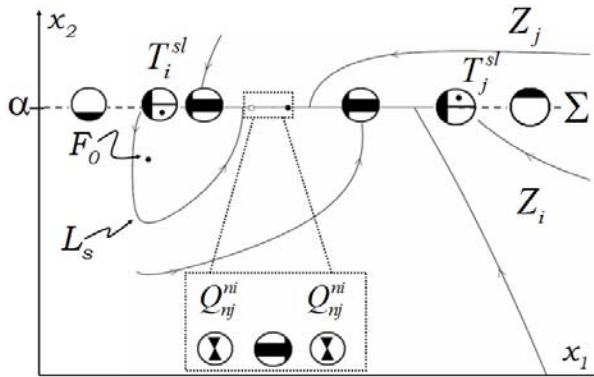
Fig. 23   State portrait of PWS prey-predator for $\alpha = 1.2375$. Stable sliding cycle and stable pseudo-node. Equation (40).

When the parameter arrives to $\alpha \approx 1.2437$ the system has a pseudo-saddle-node (PSN) bifurcation. In the equation (39) we present the sequence of points on DB in the PSN point.

$$\cdots \underset{x_{b2}=0.047}{\underbrace{T_i^{sl}}} \to S_s^l \to \underset{x_{b4}=0.3584}{\underbrace{Q_{nj}^{ni}}} \to S_s^l \to \underset{x_{b6}=0.793}{\underbrace{T_j^{sl}}} \cdots \qquad (39)$$

In $x_b=(0.3584,1.2437)$ appears a pseudo-equilibrium point Q_{nj}^{ni}. In the figure (22) we present the state portrait in the PSN bifurcation point. The transition $S_s^l \to Q_{nj}^{ni} \to S_s^l$ was explained in the section IV(7).

$$\cdots S_s^l \to \underset{x_{b4}=0.2532}{\underbrace{Q_{nj}^{ni}}} \to S_s^r \to \underset{x_{b4}=0.3813}{\underbrace{Q_{nj}^{ni}}} \to S_s^l \cdots \qquad (40)$$
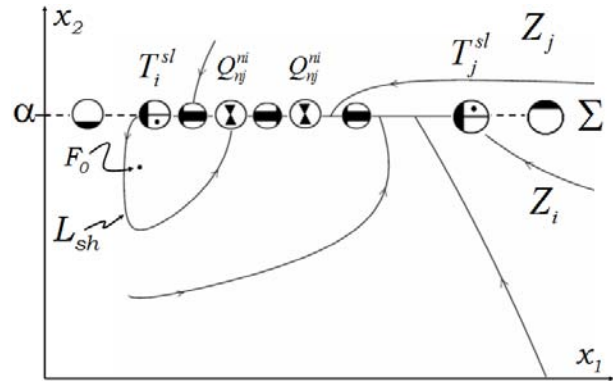

Fig. 24   State portrait of PWS prey-predator for $\alpha \approx 1.2277$. Sliding homoclinic orbit to a pseudo-saddle bifurcation.

Reducing a little the α value, the point Q becomes in two points Q just as was presented in the figure 16(d). Between the two points Q_{nj}^{ni} a sliding segment S_s^l appears. In the equation (40) we present the sequence of points on DB for $\alpha=1.2375$. Two changes of direction in the sliding segment are present in the state portrait of the figure (23).

When α is diminished, a sliding homoclinic orbit is formed at $\alpha \approx 1.2277$. In the figure 24 we present the state portrait with the cycle L_{sh}. The pseudo-homoclinic bifurcation can be detected using the SPT method verifying the equation (34).
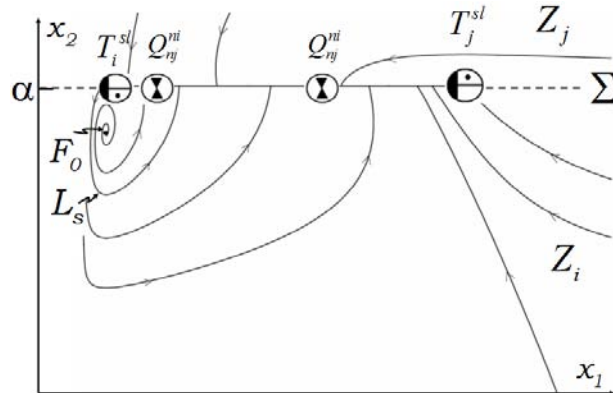

Fig. 25   State portrait of PWS prey-predator for $\alpha = 1.175$. Stable pseudo-node. Equation (41).

If the parameter α is reduced newly, the sliding homoclinic orbit disappear and a sliding cycle is formed. The sequence of points is equal to the sequence presented in the equation (40) but the pseudo equilibrium points are come closer to tangent points just as shown in the equation (41) for $\alpha=1.175$.

$$\cdots S_s^l \to \underset{x_{b4}=0.1792}{\underbrace{Q_{nj}^{ni}}} \to S_s^r \to \underset{x_{b4}=0.4912}{\underbrace{Q_{nj}^{ni}}} \to S_s^l \cdots \qquad (41)$$

The state portrait for $\alpha=1.175$ is presented in the figure 25. The sliding cycle has a S_s^r points and T_i^{sl} point on DB. Note

that the discontinuity boundary is coming closer to unstable focus F_0. This fact is reflected in the DB with the proximity of the points T_i^{sl} and Q_n^{jni}.
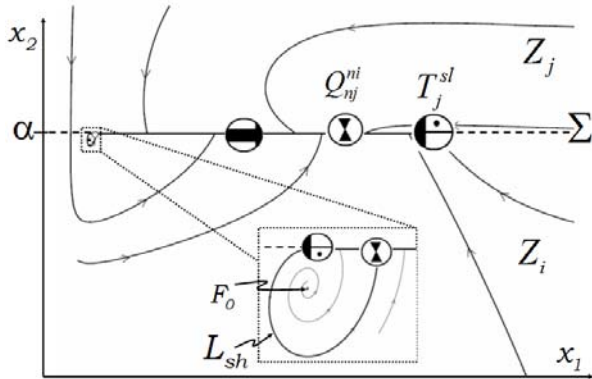

Fig. 26   State portrait of PWS prey-predator for $\alpha \approx 1.03$. Sliding homoclinic orbit to a pseudo-saddle bifurcation. Equation (42).

When $\alpha \approx 1.03$, a second homoclinic bifurcation can be detected. The cycle L_{sh} is very small due to the extreme proximity of the points T_i^{sl} and Q_n^{jni}. The location of these points is presented in the equation (42). The state portrait is presented in the figure 26.

$$C_{ji} \to \underbrace{T_i^{sl}}_{x_{b2x}=0.047} \to S_s^l \to \underbrace{Q_{nj}^{ni}}_{x_{b4}=0.0594} \qquad (42)$$

In both homoclinic bifurcations, when the cycle Lsh disappear, a sliding cycle Ls is generated when α is reduced. In the figure 27 we present the state portrait of the PWS prey-predator with α=1.02.

In $\alpha \approx 1.01017$ the discontinuity boundary collides with unstable focus taking place a Boundary-Focus Bifurcation. This scenario was explained in the Section V(1). The sequence of points on DB is different due to BF bifurcation. In the equation (43) is presented the new configuration of point after the bifurcation.
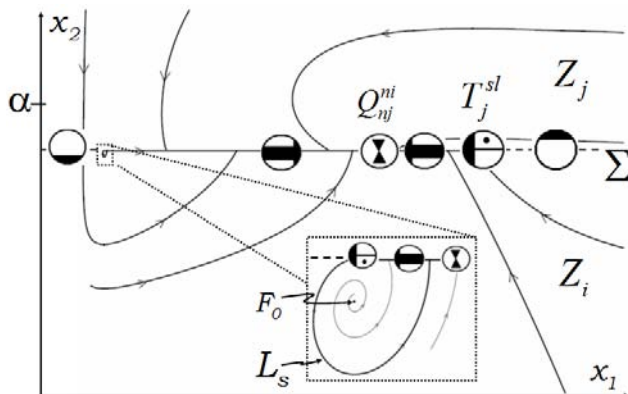

Fig. 27   State portrait of PWS prey-predator for $\alpha = 1.02$. Stable sliding cycle (almost invisible).
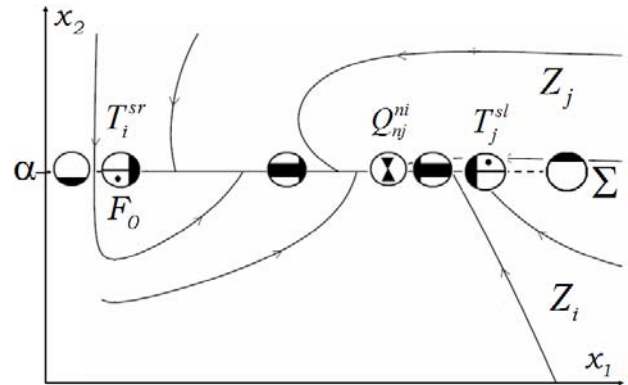

Fig. 28   State portrait of PWS prey-predator for $\alpha \approx 1.01017$. Boundary focus bifurcation. Equation (43).

$$\cdots \underbrace{T_i^{sr}}_{x_{b2x}=0.047095} \to S_s^r \to \underbrace{Q_{nj}^{ni}}_{x_{b4}=0.6235} \to S_s^l \to \underbrace{T_j^{sl}}_{x_{b4x}=0.7929} \cdots \quad (43)$$

In the figures 28 and 29 we present the state portraits for α=1.01017 and α=0.9 respectively. Only one pseudo-equilibrium point is conserved on DB. The Q_n^{jni} come closer to the tangent point T_j^{sl}.

$$C_{ji} \to \underbrace{T_i^{sr}}_{x_{b2x}=0.047095} \to S_s^r \to \underbrace{T_j^{sr}}_{x_{b4x}=0.7929} \to C_{ij} \qquad (44)$$

In $\alpha \approx 0.6527$ the pseudo-equilibrium point Q_n^{jni} collides with the tangent point in a Boundary Node (BN) bifurcation. For $\alpha < 0.6527$ the PWS prey-predator has a sequence of points on DB presented in the equation (44). Note that the sequence is similar to the sequence for $\alpha > 1.625$ presented in the equation (38) but now the sliding motion is in the other direction (S_s^r). In the figure 30 we present the state portrait for α=0.5.
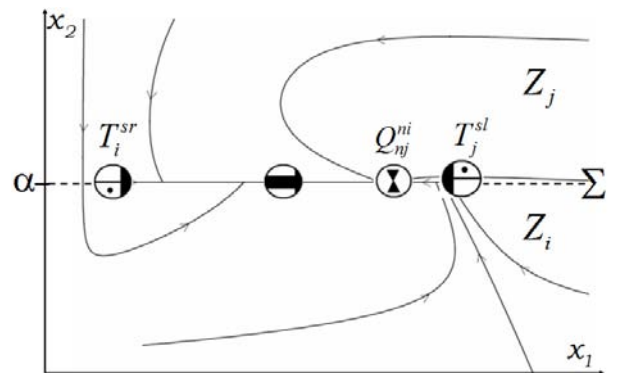

Fig. 29   State portrait of PWS prey-predator for $\alpha = 0.9$. Stable pseudo-node. Equation (43).

In the figure 31, we present the bifurcation diagram of the PWS prey-predator given by the equation (36) when α is varied in the range [3; 0.25]. Local and global nonsmooth bifurcations can be identified using SPT method.
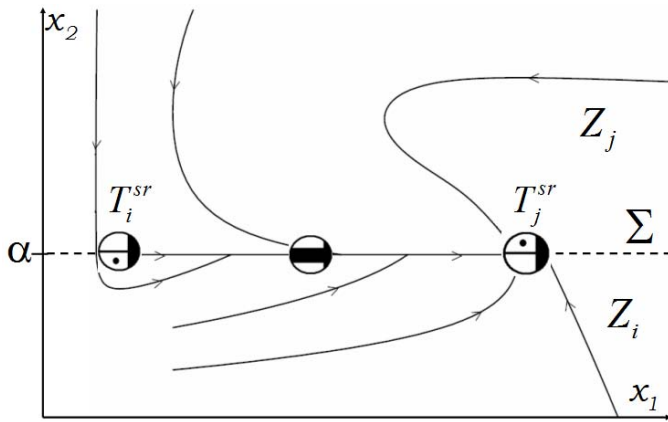
Fig. 30   State portrait of PWS prey-predator for α = 0.5. Stable pseudo-node. Equation (44).
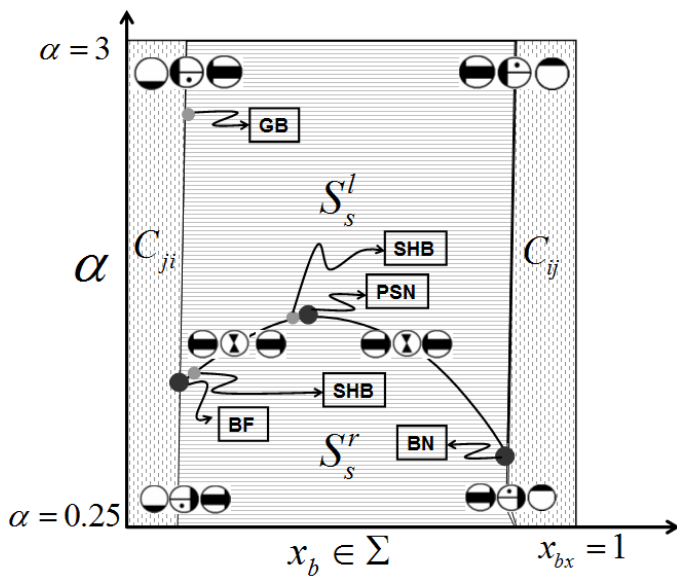

Fig. 31   Bifurcation diagram of PWS prey-predator. GB: Grazing bifurcation. PSN: Pseudo-saddle-node bifurcation. SHB: Sliding homoclinic bifurcation. BF: Boundary Focus. BN: Boundary Node.

VIII.   CONCLUSIONS AND FUTURE WORK

We have proposed a novel numerical method for continuation of nonsmooth bifurcations in Filippov systems denominated Singular Point Tracking (SPT). We have used a classification of points and events on the discontinuity boundary (DB) recently proposed. We have identified the singular points on DB for an arbitrary parameter value. Later, we have used the characterization of the singular points as initial condition in the continuation algorithm based on SPT method. Finally, we have determined the existence of nonsmooth bifurcation associated to changes in the singular point curves when a parameter is varied.   The future work is related with the application of the SPT method to three dimensional nonsmooth systems.

REFERENCES

[1]   B. Brogliato. *Nonsmooth Mechanics Models, Dynamics and Control.* Springer Verlag, New York, 1999.
[2]   M. Kunze. Non-smooth Dynamical Systems. Springer Verlag, Berlin. Lecture Notes in Mathematics, Volume 1744., 2000.
[3]   Leine R.I. H. Nijmeijer. Dynamics and Bifurcations in Non-Smooth Mechanical Systems. Springer Verlag, 2004.
[4]   R. I. Leine. *Bifurcations in Discontinuous Mechanical Systems of Filippov¡Type*. PhD thesis, Technische Universiteit Eindhoven, 2000.
[5]   I. Merillas. Modelling and numerical study of Nonsmooth Dynamical Systems. PhD thesis, UPC Doctorate programme in Applied Mathematics, 2006.
[6]   C. J. Budd M. di Bernardo and A. R Champneys. Grazing and border-collision in piecewise smooth systems: a unified analytical framework. *Phys. Rev. Lett*, 86:2553,2556, 2001.
[7]   U. Galvanetto. Some discontinuous bifurcations in a two-block stick-slip system. *Journal of Sound and vibration*, 248(4), 653-669, 2001.
[8]   Albert C.J. Luo. A theory for non-smooth dynamic systems on the connectable domains. *Communications in Nonlinear Science and Numerical Simulation*, 10 1-55, 2005.
[9]   P. Kowalczyk and M. di Bernardo. Two-parameter degenerate sliding bifurcations in filippov systems. *Physica D-Nonlinear Phenomena*, 204(3-4):204229, May 2005.
[10] A B Nordmark. Existence of periodic orbits in grazing bifurcations of impacting mechanical oscillators. *Nonlinearity*, 14 : 15171542, 2001.
[11] G.W. Luo Y.L. Zhangb, J.N. Yua. Dynamical behavior of vibro-impact machinery near a point of codimension two bifurcation. *Journal of Sound and Vibration*, 292 242-278, 2006.
[12] B. Brogliato. *Impacts in Mechanical Systems Analysis and Modelling.* Springer Verlag, New York. Lecture Notes in Physics, Volume 551., 2000.
[13] F. Dercole, A. Gragnani and S. Rinaldi. Bifurcation Analysis of piecewise smooth ecological models. Theoretical Population Biology. 72 (2007) 197-213.
[14] F. Dercole, A. Gragnani, R. Ferriere and S. Rinaldi. Coevolution of slow-fast populations. An application to prey-predator systems. Proc. R. Soc. London B.273, 983-990, 2006.
[15] A. F. Filippov. Differential equations with discontinuous righthand sides. *Kluwer Academic Publishers*, Dortrecht, 1988.
[16] Yu. A. Kuznetsov S. Rinaldi, A. Gragnani. One¡parameter bifurcations in planar Filippov systems. *International Journal of Bifurcations and Chaos*, 13(8):21572188, 2003.
[17] P. Mosterman and G. Biswas. A theory of discontinuities in physycal system models. *El Sevier*, 325B, 1998.
[18] Sven Hedlund. *Computational Methods for Hybrid Systems*. PhD thesis, Lund Institute of Technology, 1999.
[19] P.T. Piiroinen Yu. A. Kuznetsov. An event-driven method to simulate filippov systems with accurate computing of sliding motions. Technical report, University of Bristol, 2005.
[20] F. Dercole Yu. A. Kuznetsov. User Guide to Slidecont 2.0. Department of Mathematics, Utrecht University. The Netherlands. 2004.
[21] F. Dercole Yu. A. Kuznetsov. Slidecont: An auto97 driver for bifurcation analysis of filippov systems. ACM Trans. Math. Softw, 31, 95 - 119, 2005.
[22] I. Arango J. A. Taborda. Nonsmooth analysis methodology on discontinuity boundary of Filippov systems. *submitted to IJBC*, 2008.
[23] I. Arango and J. A. Taborda. Analyzing Sliding Bifurcations On Discontinuity Boundary of Filippov Systems. *Proceedings of the American Conference on Applied Mathematics (MATH 08)*, 2008.
[24] I. Arango and J. A. Taborda. Characterizating points on discontinuity boundary of Filippov systems. *Proceedings of IASTED International Conference on Modelling, Identification and Control (MIC 2008)*, 2008